sustainability

MDPI

Article

Flexible Multifunctional Self-Expanding Electrospun Polyacrylic Acid Covalently Cross-Linked Polyamide 66 Nanocomposite Fiber Membrane with Excellent Oil/Water Separation and High pH Stability Performances

Jiangyi Yan [1], Lihong Nie [1], Guiliang Li [2], Wenxin Wu [3], Ming Gao [4], Yuanlu Zhu [4], Weixing Wu [1] and Beifu Wang [1,*]

[1] College of Petrochemical Engineering and Environment, Zhejiang Ocean University, Zhoushan 316000, China
[2] Sinopec Zhongyuan Oilfield Company, Petroleum Engineering Technology Research Institute, Puyang 457000, China
[3] The Fourth Branch of China Petroleum Pipeline Engineering Co., Ltd., Langfang 065000, China
[4] China College of Naval Architecture and Shipping, Zhejiang Ocean University, Zhoushan 316000, China
* Correspondence: wangbeifu@zjou.edu.cn

Abstract: In this paper, we report for the first time the successful formation of a covalent cross-linking structure between polyacrylic acid and polyamide 66 in an electrospun nanofiber membrane by the facilitated amidation reaction using N-Hydroxy-succinimide (NHS) and N-(3-Dimethylaminopropyl)-N′-ethyl-carbodiimide hydrochloride (EDC). The structure and properties of the fiber membrane are characterized using scanning electron microscopy, wide field X-ray diffraction and differential scanning calorimetry. The results show that the presence of the cross-linked structure not only affects the construction of the nanofiber network framework but also influences the pore size distribution and size of the fiber membrane surface, which in turn affects its retention of contaminants and water absorption performance. After modification, the cross-linked membranes exhibited a significant retention performance of up to 77% for methyl tert-butyl ether (MTBE) with a reduced pure water flux. Furthermore, after crosslinking, the fiber membrane has been strongly enhanced with more stable pH response behavior.

Keywords: electrospinning; crosslinking modification; dense layer; expansibility; pH-responsive

check for updates

Citation: Yan, J.; Nie, L.; Li, G.; Wu, W.; Gao, M.; Zhu, Y.; Wu, W.; Wang, B. Flexible Multifunctional Self-Expanding Electrospun Polyacrylic Acid Covalently Cross-Linked Polyamide 66 Nanocomposite Fiber Membrane with Excellent Oil/Water Separation and High pH Stability Performances. *Sustainability* **2022**, *14*, 14097. https://doi.org/10.3390/su142114097

Academic Editor: Changhyun Roh

Received: 30 September 2022
Accepted: 26 October 2022
Published: 28 October 2022

Publisher's Note: MDPI stays neutral with regard to jurisdictional claims in published maps and institutional affiliations.

Copyright: © 2022 by the authors. Licensee MDPI, Basel, Switzerland. This article is an open access article distributed under the terms and conditions of the Creative Commons Attribution (CC BY) license (https://creativecommons.org/licenses/by/4.0/).

1. Introduction

Unlike conventional spinning processing techniques, electrostatic spinning is a direct and continuous method for preparing polymer nanofibers by traction and deformation of nanofibers by electrostatic forces, which can spin polymers such as polyamide, polyethylene and polyacrylonitrile into ultrafine fibers with diameters in the micron and even nanometer range [1–3]. The obtained electrospun nanofiber membranes are characterized by high porosity and low permeation resistance, and their large specific surface area also allows them to have many special functions and have broad application prospects in the fields of food, biomedicine [4], energy technology, clean water, etc. [5,6].

As we know, the open pore structure of the surface and the large pore size of the nanofiber membrane lead to poor filtration accuracy and even to the inability to achieve retention of specific substances. This requires functionalization of the fibers to obtain specific favorable results, making them ideal composite material candidates for the removal of various contaminants.

Changes in the physical properties and structure of the fibrous membrane can be induced by physical or chemical treatment of the polymer material to achieve the purpose of improving filtration efficiency and reducing resistance pressure drop [7]. In order to achieve the retention interception effect covering the whole membrane space, fillers can be

added to fill the polymer matrix. For example, Lu et al. anchored graphite nanosheets into electrospun PA66 nanofibers with porous structure to build a sensitive three-dimensional network, and the filling of carbon-based fillers further enhanced the mechanical stability of the membrane [8].

Or covalent, ionic or hydrogen bonds are formed in polymer chains to strengthen inter-chain bonds, e.g., Huang et al. attached different amounts of acrylic acid (AA) to the surface of PCL nanofibers by forming a chemically grafted bonding structure through compatibilizers and photo-initiators, which improved the hydrophilicity of the fibers [9]. Therefore, the appearance of high permeation and retention is often accompanied by two factors: on the one hand, the relative closure of the surface macropores provides a dense and continuous protective layer; on the other hand, the existence of tiny pores inside the membrane still provides a channel for the passage of large numbers of water molecules.

Polyamide 66 can be an excellent material for nanofiber membranes due to its high tensile strength and impact resistance in ensuring high membrane stability [10]. These favorable properties make PA66 suitable for the preparation of wettable porous fiber membranes and are prospective for applications in separation processes. Similarly, PAA, as a highly functional polymer, can achieve the regulation of a variety of physical properties through chemical treatment that can be used as a modifier for electrospun fibers while improving the flexibility of electrospun nanofibers [11].

Converging a large number of hydrophilic groups on the fiber surface or improving the density of membrane pores are considered the two most commonly accepted modification methods. Based on the aforementioned ideas, polyacrylic acid was used to modify the polyamide 66 nanofiber membrane to improve its mechanism and microstructure. The combination of the amidation promoter NHS and EDC improved the cross-linking efficiency of the carboxy-amine system [12].

In this paper, the effects of amidation cross-linking on the separation and retention properties, the associated swelling and stability of PAA/PA66 electrospun nanofibers were investigated. The aim is to prepare a new type of nanofiber membrane with strong pollutant separation performance. The chemical composition, microstructure and separation and interception performance of the nanofiber membrane were studied and analyzed by various analysis methods.

2. Experimental

2.1. Materials

Polyamide 66 (PA66, A.R) was provided by French manufacturer Rhodia Co., Ltd., Bangkok, Thailand. Formic acid (HCOOH, FA, 94%) was purchased from Yangzi Petrochemical Basf Co., Ltd., Nanjing, China. Poly(acrylic acid) (PAA) (average Mv~3 kDa) (Solid content of 30%) was obtained from RON ss chemical reagent. N-(3-Dimethylaminopropyl)-N′-ethyl-carbodiimide hydrochloride (EDC), N-Hydroxy-succinimide (NHS) and Methyl tertiary butyl ether (MTBE) were obtained from Aladdin Chemical Reagent. Phosphate buffer solution (PBS) was received from Xiamen Anyongbo Technology Co., LTD (China). Hydrochloric acid (HCl), sodium hydroxide (NaOH), potassium chloride (KCl) and sodium chloride (NaCl) were supplied by Sinopharm Chemical Reagent Co., Ltd. All chemicals and solvents were used as received.

2.2. Preparation of Electrospun PAA-PA66 Nanofiber Membranes

PA66 was dissolved in formic acid under a magnetic stirrer at 60 °C until a clear homogeneous solution was formed with a concentration of 15 wt%. The solution was naturally cooled to room temperature. Then, PAA pure solution and the as-prepared PA66 solution were mixed with a polymer mass ratio of 1:3. The resulting mixture was further stirred at room temperature for 1 h to obtain a homogeneous solution for electrospinning.

In order to remove excess air bubbles within the polymer solution, the solution was subjected to 20 min of ultrasonication. Next, the mixture was fed into a 10 mL syringe with a stainless steel needle. The positive electrode wire was hooked at the metal part

of the needle and negative part of the electrode was attached to the high-speed drum collector. The electrospinning system was carried out at certain conditions (humidity: 45%, temperature: 28 °C). Table 1 summaries the operating conditions of the electrospinning system in this work. The collected blended electrospun fiber membranes were dried in a vacuum oven at 25 °C for 24 h. The preparation process diagram for nanocomposite fiber is shown in Figure 1.

Table 1. Operating conditions of the electrospinning process in this work.

Parameter	Value
Positive-voltage	29.6 KV
Negative-voltage	2.4 KV
Spinneret to rotary collector distance	8 cm
Sliding table speed	20 mm/min
Collector rotation speed	50 rpm

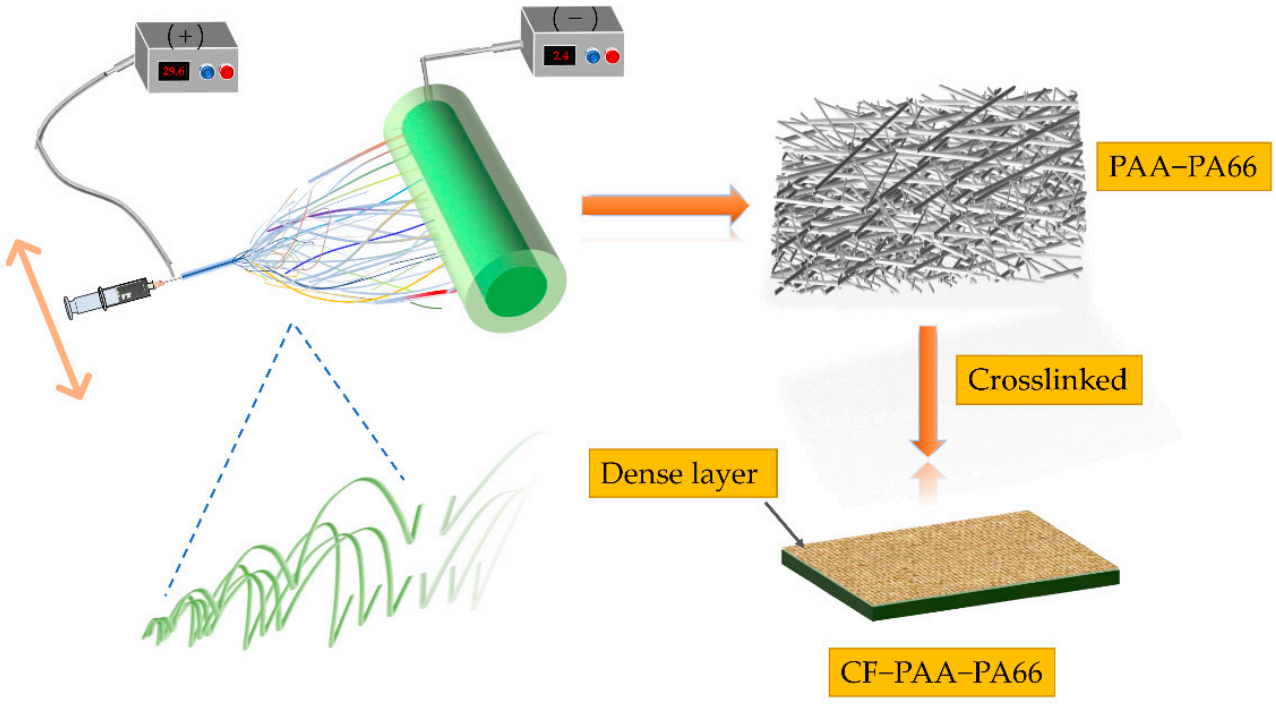

Figure 1. Schematic diagram of the electrospinning process.

2.3. Polymer Crosslinking (CF-PAA-PA66)

The electrospun nanofiber membrane was pre-immersed in phosphate buffer solution (PBS) (pH = 5.8) for 15 min, adding the pre-weighed NHS into the PBS solution, gently stirring and waiting for 10 min, and finally adding the pre-weighed EDC. Molar ratios of NHS and EDC to the carboxylic acid groups of PAA varied from 0.25 to 2 and 1 to 3, respectively. After that, the reactants were incubated at 50 °C for 24 h with gentle stirring. After the reaction, the membrane was thoroughly cleaned several times with deionized water and ethanol to remove unreacted NHS and EDC, and dried in a vacuum oven at 25 °C for 24 h before further characterization. The as-prepared sample was named CF-PAA-PA66.

An overview of the basic and functional nanofibers prepared by electrospinning is shown in Table 2. Under the condition of high levels of crosslinking, the optimum value of fiber comprehensive stability can thus be obtained.

Table 2. Summary of research on the electrospun nanofiber membranes.

NanofiberPolymer	Modified Additive	Functionalization Method	Advantages	Application	Ref
PAA	1,4-butanediol di-glycidyl-ether	Esterification reaction	High swelling rate, high water absorption	The diaper and napkin	[13]
PA66	_____	_____	PA66 bundles arranged with different nanofibers	_____	[14]
PAA	β-cyclodextrin	Heat-induced crosslinking	Forming ester bond to improve water resistance of PAA fiber, strongly pH-responsive swelling behaviors	_____	[15]
PA66	Graphite nanosheet (GN)	Immersed in the GN suspension	A multifunctional sensor, the excellent multifunctional response for strain, temperature and gas sensing	The detection of human motion and physiological ECG signal	[8]
PAN	PDA	The spin coating	Increase the stress strength, high electrolyte uptake, high ionic conductivity, wide electrochemical window	Lithium ion battery for energy storage systems	[16]
PVA/PAA	PDA	Thermal crosslinking + Dopamine self-polymerizing coating	Efficient adsorption performance toward methyl blue, highly flexible, easy to operate and retrieve, easy to elute and regenerate	Wastewater treatment	[17]
PA66	PAA	Amide crosslinking	Contains dense layer, high water absorption, high rejection rate, high heat stability	Oily sewage treatment, cleaning alternative items	This work

2.4. Membrane Characterizations

The morphology and microstructure of the fibers were observed using scanning electron microscopy (SEM Gemini 300, ZEISS, Jena, Germany) with an accelerating voltage of 15 kV. Before observation, all samples were treated with Au/Pd sputtering and carefully handled to avoid contamination.

X-ray photoelectron spectroscopy (XPS Thermo Scientific K-Alpha, Waltham, MA, USA) was used to investigate the surface chemical compositions of nanofiber membranes. The range of survey spectra is from 0 to 1300 eV and the C1s peak of high-resolution spectra were detected.

Fourier transform infrared spectroscopy-attenuated total reflectance (FTIR-ATR) measurement was carried out using a Thermo Scientific Nicolet iS20 Fourier transform infrared spectrometer. The samples were placed on the sample holder and all spectra were recorded from 4000 cm^{-1} to 600 cm^{-1}.

The crystal structure of polyamide 66 in the prepared electrospun PA66 nanofiber membranes was determined by means of a wide-angle X-ray diffractometer (WAXD, Rigaku Smartlab 9 KW, Tokyo Akishima, Japan) with λ (1.54 Å, Cu Kα line) at a generator voltage of 40 kV and a generator current of 40 mA.

Melting behavior of PA66 nanofiber membranes were studied using a differential scanning calorimeter (DSC 200-F3, NETZSCH, Germany) in a nitrogen atmosphere. About 8 mg of dry fiber was sealed in an aluminum pan. It was kept at 20 °C for 3 min, then heated to 600 °C at a heating rate of 10 °C/min and maintained for 3 min to remove the thermal history, and then chilled to 20 °C (the rate of 10 °C/min), during which the melting curves were recorded. All tests were carried out under a dry nitrogen atmosphere at a pressure of 0.05 MPa and the flow rates of purge gas and protective gas were 40 mL/min and 60 mL/min, respectively.

In addition, thermogravimetric analysis (TGA) was performed on a TGA Instruments HCT-1 thermal analyzer at a heating rate of 10 °C/min.

Thermal stability and shrinkage of the relevant fibers were measured by heat treating them in an oven at 200 °C for 0.5 h.

2.5. Water Content

The fiber membranes with an area of 1 cm^2 were placed in a closed flask with 100 mL of deionized water and allowed to stand for 24 h at room temperature. The excess water on the surface of the wet fibers was removed with filter paper and weighed. After that, they were dried in an oven at 60 °C and weighed once again. The average was made by measuring in parallel three times for each sample. From the results obtained from weighing the samples in wet and dry conditions, the amount of water absorbed by the membrane was calculated with the equation:

$$water = \frac{Ww - Wd}{Wd} \times 100\% \quad (1)$$

where Ww is the weight of wet membranes (g) and Wd is the weight of dry membranes (g).

2.6. The Overall Pore Volume of Fibrous Membranes

The ability of electrospun fiber membranes to maintain low surface tension allows its overall pore volume to be evaluated by the capacity to absorb low-viscosity liquids. After measuring the dry weight of the membranes, they were immersed in n-butyl alcohol for 12 h to become wet, and the wet weight was then measured. The overall pore volume of fibrous membranes was obtained by the following equation:

$$Cv = \frac{[(Wh - Wd)/\rho]}{Wd} \quad (2)$$

where Wd and Wh are the membrane mass before and after the immersion, respectively, and ρ is the density of n-butyl alcohol.

2.7. The Hydrophilicity of Nanofiber Membranes

The hydrophilicity of fibrous membranes was observed based on the water contact angle measurement (WCA). The WCA of the membrane was measured using an optical contact angle tester (OCA15Pro, DataPhysics Instruments GmbH, Filderstadt, Germany) according to the sessile-drop method. This contact angle can be described as an angle between the sample surface and calculated drop shape function, the projection at which the drop image is referred to as the baseline. The average was made by measuring parallelly three times for each sample.

2.8. Swelling Experiments

The 10 mg sample was immersed in PBS buffer solutions of different pH at 30 °C for 24 h, after which the excess solution on the surface was removed and weighed to study the swelling ratio of the blended and crosslinked fiber membranes. HCl and NaOH were used to adjust the pH of the solution. The swelling ratio (q) was calculated by the following equation:

$$q = \frac{Ww - Wi}{Wi} \quad (3)$$

where Wi and Ww were the mass of the sample before and after immersion, respectively.

The equilibrium swelling ratio test was carried out in order to further check the swelling and water absorption properties of the fiber membrane. This experiment is also based on the quantitative characterization of swelling degree. Each 50 mg of fiber was immersed in 100 g of deionized water, 0.9 wt% sodium chloride, and potassium chloride solutions, and the mass after expansion and absorption was weighed at different time intervals. Until the stable equilibrium swelling ratio of the fiber membrane was

obtained. The absorbed water ratio of the fiber membrane was calculated using the following equation:

$$AW = \frac{Ws - Wd}{Wd} \times 100\% \quad (4)$$

where Wd and Ws are the initial and expanded weights of fiber membrane samples, respectively.

Interestingly, the increase of wet weight at different culture periods in PBS solution can also be used to measure the swelling degree of the fiber membrane, and the polymer expansibility and adhesion to salt ions of PA66 electrospun fiber membrane materials in different incubation environments can also be further explored. The fiber membranes of the same size were taken and their initial weight (Wi) was measured, after which they were immersed in phosphate buffer solution (pH = 5.8) and kept in closed culture tubes at 37 °C for 3, 5, 10, 24, 34, 48, 58, and 72 h. After the°orresponding specified time, the sample was removed and the surface solution was removed with filter paper. The wet weight (Ww) was then weighed. After drying at room temperature for 24 h, the weight was weighed again to be the dry weight (Wd). The corresponding swelling percentage can be calculated by the following equation

$$Swelling = \frac{Ww - Wd}{Wi} \times 100\% \quad (5)$$

2.9. Nanofibers Performance Tests

Nanofiber performances were evaluated by the pure water flux and MTBE rejection effect. The pure water flux test was used to express the permeability of the fiber membrane. This was carried out under the negative pressure of 0.1 MPa. The flux was equilibrated for the passage of the first 30 min permeate whilst the following 10 min permeate was collected. For the rejection experiments, infrared spectrophotometer (JLBG-126+) was employed to analyse the concentration of the feed solution and permeation of the MTBE solution. The feed solution was 1 g/L MTBE solution. The filtered solution was obtained in the same way as water flux testing. The water flux (J), MTBE rejection (R) were determined by the equations as follows:

$$J = \frac{V}{A \cdot \Delta t} \quad (6)$$

$$R = \frac{CF - CP}{CF} \times 100\% \quad (7)$$

where J is pure water flux (L/(m^2·h)), V is the volume of penetrated water (L), A is the effective area of the membrane (m^2) and Δt and is the recorded time (h). R is the percentage retention rate or MTBE rejection, CF is the concentration of feed solution and CP is concentration of permeation.

2.10. Mechanical Property of Nanofiber Membranes

The microcomputer controlled electronic universal testing machine (CMT8501, China) was employed to determine the mechanical property for PA66 nanofiber membranes by measuring the stress–strain curve. Each sample was tested at least three times to obtain an average strength.

3. Results

3.1. Morphology and Structure of Nanofiber Membranes

The morphology of PAA/PA66 blend and crosslinked spinning fiber membranes were visualized by SEM (Figure 2). From the SEM images presented in Figure 2a, it can be observed that various nanofibers of varying thickness overlap and twist around each other, weaving to form a mesh-like porous membrane. In principle, the density reversibility and coverage of the PA66 nanofiber network can be changed by adjusting the deposition time of electrospinning [18].

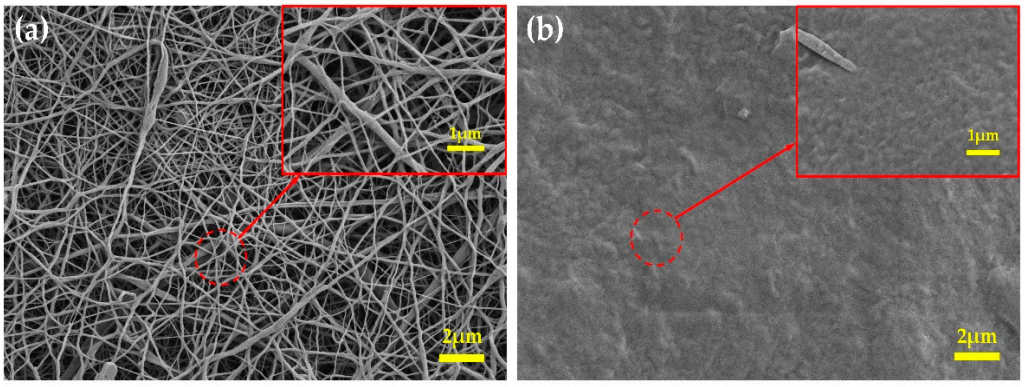

Figure 2. SEM image of the original PAA/PA66 blended spinning membrane (**a**), PAA-PA66 fiber membrane after amidation and crosslinking (**b**).

Due to its high strength, stiffness and good impact resistance, the PA66 spinning fiber as a matrix provides sufficient mechanical strength for the formation of the network structure and greatly improves the stability and flexibility of the overall membrane [8]. PAA fibers, as functionalized modifiers, not only serve as fillers interspersed in the porous network architecture but also provide hydrophilic active groups on the surface of nanocomposites [19].

In addition, it can be clearly seen that the fibers are asymmetrical. What is more interesting is that there are some tiny microcrystalline fibers with random distribution adhering to the surface of each fiber and showing a certain sprouted crystal shape, which is perhaps due to the presence of strong hydrogen bonds in the aqueous PAA solution, allowing a small portion of droplets to be ejected directly from the spinneret to the collector, increasing the solvent concentration on the collection drum [20].

However, for PAA cross-linked PA66 fiber membrane, as shown in Figure 2b, the fibrous mesh structure disappeared and a relatively non-porous dense layer was formed on the membrane surface, which was beneficial to increasing the retention resistance and improving the rejection effect on contaminants. On the one hand, this is due to the obvious amidation reaction between PAA and PA66, which blocked the original porous channel structure on the membrane surface; on the other hand, perhaps because of the rapid cross-linking of PAA and PA66 on the membrane surface at the interface of the two phases under the action of the cross-linking agent, the rapid coagulation occurred at the same time [21].

The mechanism of the amidation cross-linking reaction between PAA and PA66 is shown in Figure 3, in which NHS and EDC are amidation promoters.

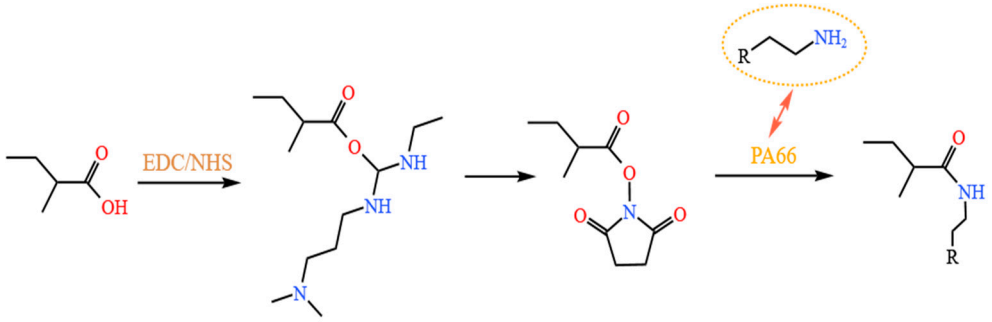

Figure 3. Diagram of the formation mechanism of PAA/PA66 cross-linked amidation.

3.2. Chemical Characterizations

Fourier transform infrared spectroscopy (FTIR) was used to analyze chemical composition changes on the surface of the PA66 nanofiber membranes (Figure 4) [22]. The FTIR curves of the two membranes are almost identical due to their similar chemical structures.

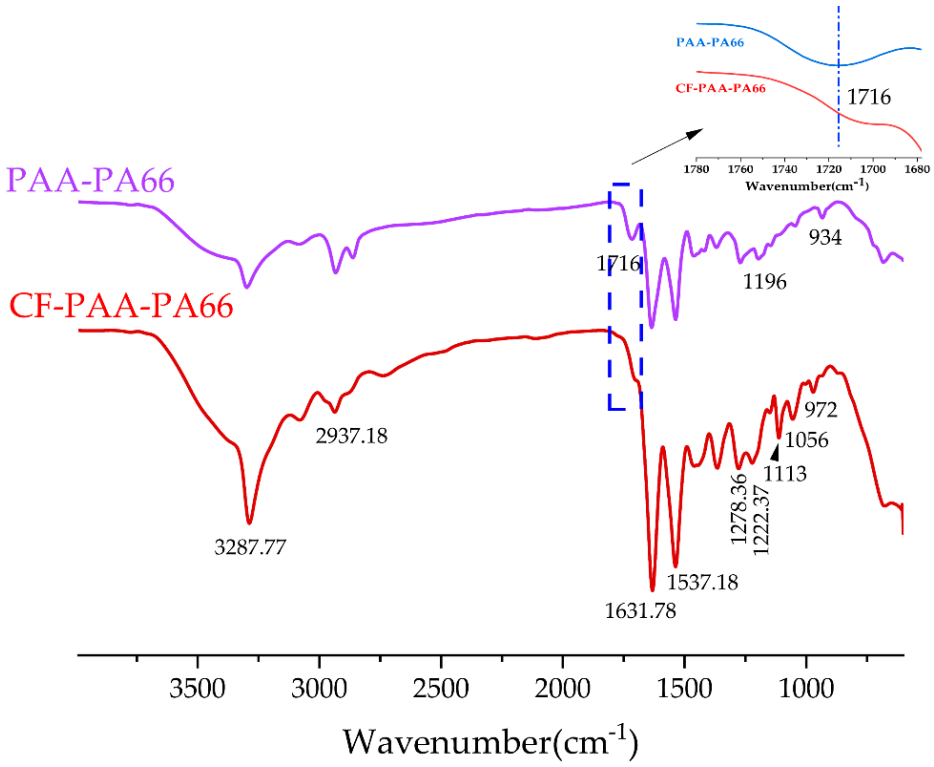

Figure 4. FTIR spectra of PAA/PA66 fiber membranes before and after crosslinking modification.

Taking the cross-linked fibrous membrane as an example, the spectrum shows the existence of N-H stretching vibration (3287.77 cm^{-1}), N-H shear vibration and C–N stretching vibration (1537.18 cm^{-1}); C=O stretching vibration (1631.78 cm^{-1}). The characteristic peaks at 2937.18 cm^{-1} correspond to the stretching vibration of methylene (-CH_2). Furthermore, small peaks at 1310–1200 cm^{-1} correspond to C-N stretching vibration and N-H shear vibration in polyamide [23].

However, it is noteworthy that after the replacement of the oxygen in the carboxyl group by the amino group, the symmetric and antisymmetric vibration peaks of C=O in PAA (1716 cm^{-1}) and the stretching vibration peak of C-N in the amino group of PA66 (1196 cm^{-1}) in the PAA-PA66 fiber membrane disappear obviously. By contrast, new C-N stretching vibration peaks appear at 1113 cm^{-1} and 1056 cm^{-1} in the CF-PAA-PA66 membrane, which is due to the formation of new amide groups and the weaker electron donating ability of nitrogen than oxygen. Since the number of carboxyl groups in PAA is fixed, we can also conclude that the cross-linking reaction between carboxylic acid and amine is complete. In addition, the infrared peak representing the crystallization region changed from 934 cm^{-1} to 972 cm^{-1} under the influence of crosslinking, indicating that the crystal form of PA66 changed to some extent before and after crosslinking; The absorption peak in CF-PAA-PA66 shifts to a higher wave number, which indicates that the hydrogen bond interaction force in PAA/PA66 is weakened.

3.3. Crystalline Structure

In order to further obtain information related to the polymorphisms of PA66 fiber membranes in this study, XRD measurements were carried out. Figure 5 shows the diffraction patterns of two PA66 fiber membranes. There are two diffraction peaks at 2θ values of about 20.2 and 23.9, which correspond to crystal types α1 (100) and α2 (010/110) of PA66, respectively, proving that crystal type α is formed during the process of fiber membrane spinning and deposition.

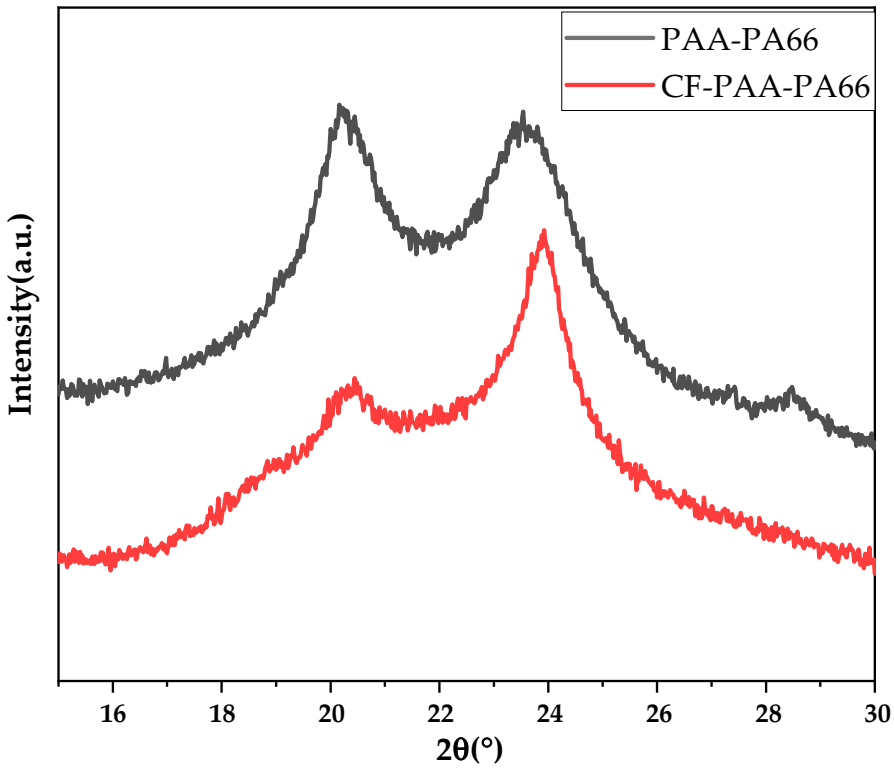

Figure 5. X-ray diffraction patterns of different fibrous membranes.

Notably, the diffraction peak of α2 crystal in the CF-PAA-PA66 fiber membrane exhibits significant narrowing and enhancement, which indicates that a large number of α2 crystals are occupied in the formed membrane, which further reduces the distance between α2 sheet crystals in PA66 without external force. The formation of a large number of α2 crystals may be due to the transformation of more α1 crystals into α2 crystals during the cross-linking chemical process. The diffraction peaks of α1 crystals in PA66 are basically unchanged [24].

With the decrease of α2 grain size in the cross-linked membrane, the crystallinity of PA66 in the membrane decreases, which is consistent with the subsequent analysis results obtained by DSC.

3.4. Thermal Stability

The DSC curves of the two fiber membranes are shown in Figure 6a. A broad endothermic peak (20–130 °C) can be observed in both curves during the heating process, followed by an obvious Brill transition peak at 242 °C for the PAA-PA66 membrane, while the Brill transition peak of PA66 in the cross-linked membrane disappears. The Brill transition is related to the deformation of the crystal, which is the equilibrium point for the structural transformation of the crystal. Below this temperature, the crystal exhibits a triclinic structure, otherwise a pseudo hexahedron.

In polyamide crystals, the cell movement and the alignment position between the cells are hardly affected by temperature, but the slip between the planes varies with temperature. Therefore, the Brill transition can be attributed to the slip between the sheet crystals.

In the PAA-PA66 fiber membrane, the slip between the polyamide sheet crystals is bound by hydrogen bonding, which occurs not only between the molecular chains of PA66 itself but also between the chains of the two different polymers. After the formation of a new amide structure with PAA, the binding effect on the molecular chain segments of PA66 is enhanced, further hindering the slip of the sheet crystals.

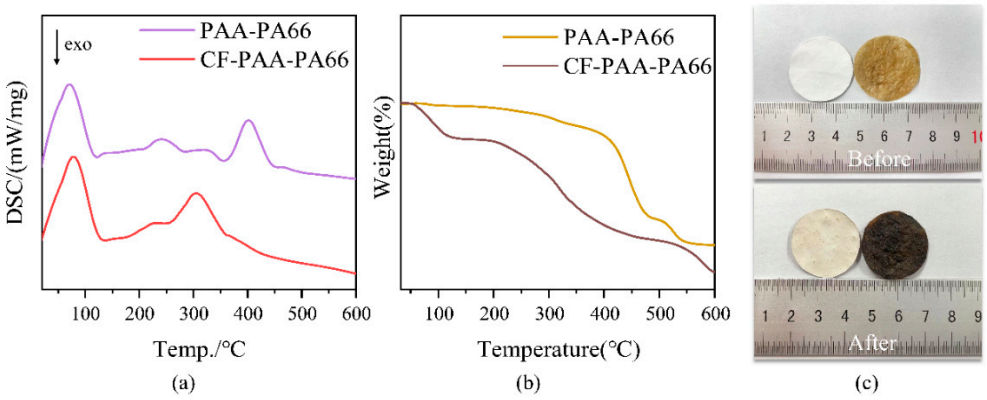

Figure 6. Characterization results of thermal stability of fiber membranes. (**a**) DSC curve. (**b**) TG curve. (**c**) Changes influenced by temperature.

TG profiles of different fiber membranes are shown in Figure 6b. As can be seen from the figure, the thermal decomposition curve of PAA-PA66 fiber membrane shifted rightward with two weight loss steps, which involved a two-step decomposition reaction. The weightlessness temperature starts at 384 °C and ends at 584 °C. The breakage of polyamide 66 chain segment mainly occurs between the amide bond and carbon and nitrogen bonds, while the breakage of the polyacrylic acid chain segment mainly occurs in the carboxyl group. Combined with the literature, we speculated that the first step is the breakage of amide bonds, carbon and nitrogen single bonds and the occurrence of decarboxylation in PAA, and the second step is the decomposition and oxidative volatilization of the cleavage product [25].

Instead, the CF-PAA-PA66 fiber membrane involves three stages of weight loss. In the first stage, a small part of weight is lost, which may be due to the loss of a small amount of water contained in the sample, which is related to the high moisture absorption property of the cross-linked membrane itself. In the second step, the amide bond and carbon-nitrogen single bond are also broken. As the newly formed unstable covalent amide bond is easily broken preferentially at high temperature, so the thermal decomposition rate is reduced to a certain extent. The third step is basically the same as the final trend of PAA-PA66 fiber membrane [26].

Figure 6c depicts images of the related fiber membranes after heat treatment. After heating, the color of both membranes deepened, which is due to a certain degree of oxidation in the presence of heat and air, and the degree of oxidation of the cross-linked fiber membrane is greater, whereas they all have a shrinkage rate of less than 5.6%, which means that the relevant fiber membranes have excellent resistance to denaturation and rigidity [16].

3.5. Water Content, Overall Pore Volume, and Contact Angle

The characterization of water content of fibrous membranes can not only show the porosity of membranes but also support the results of the morphological structure of the membranes. PAA-PA66 fiber membrane has greater water absorption, which is directly related to its large porosity and the strong hydrophilicity of the carboxyl group in PAA [21]. However, the lower water absorption content of the CF-PAA-PA66 fiber membrane correlates with the dense layer on the surface, as observed by SEM.

Through the comparison of the total pore volume test, the retention effect of the blended fiber membrane on n-butanol was more than twice that of the cross-linked fiber membrane, which is probably due to the cross-linked structure in the cross-linked fiber acting as a proper site barrier and weakening the polymer chain activity [15].

The static water contact angles of the two fiber membranes shown in Figure 7b indicate that the occurrence of cross-linking reaction does not change their hydrophilic properties. The PAA-PA66 membrane has a lower contact angle, which is attributed to the presence

of a large number of hydrophilic carboxyl groups on its surface. While CF-PAA-PA66 membrane has amide groups, the good wettability of the material also enables the water droplets to spread out on the surface.

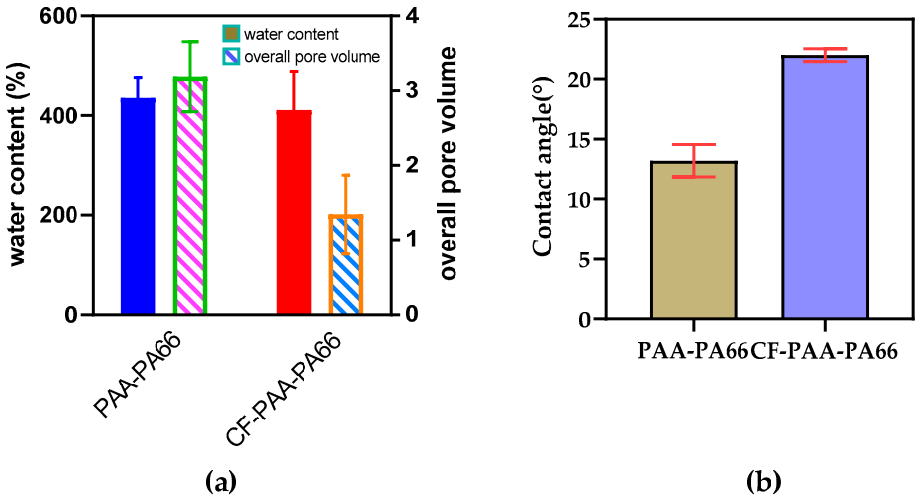

Figure 7. Physical characterization parameters of nanofiber membranes: (**a**) water content and overall pore volume; (**b**) contact angle.

3.6. Equilibrium Swelling Performance and pH-Responsive Swelling Behavior

The pH-responsive swelling behavior of the two fiber membranes in pH buffer solution is shown in Figure 8. Their swelling ratios both showed a trend of increasing and then decreasing, with a shift around PH = 7. When pH < 7, with the increase of pH of buffer solution, carboxylic acid groups in PAA and free groups at the end of PA66 chain segments in the fiber membrane dissociate, making the osmotic pressure inside the fiber higher than that of the surrounding solution, resulting in the surrounding solution flowing into the fiber and fiber expansion [15]. This indicates that the fibers respond well to H+ ions in solution under sufficient wetting conditions. When pH > 7, the negative charge repulsion between the carboxylic acid base group and the OH_ ion in the PAA-PA66 fiber membrane increases, and the diffusion of the solution into the fiber is hindered, which increases the flow resistance. However, the decrease in the cross-linked membrane trend is due to its own low pore density.

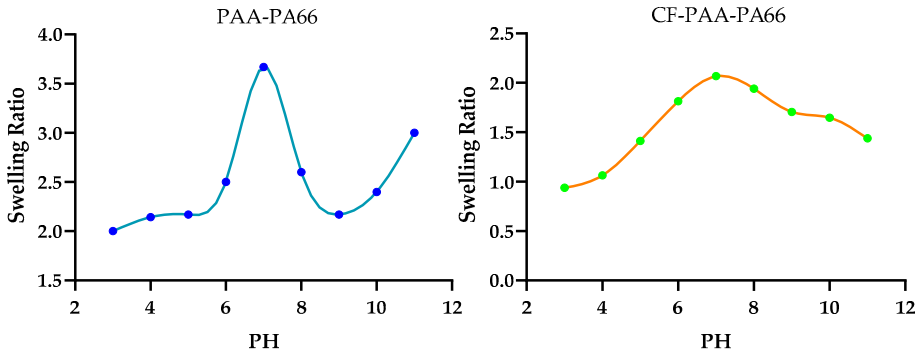

Figure 8. pH responsive behavior of nanofiber membranes.

The embedding of water in the matrix upon contact of nanofibers with water enhances the expansion of the membrane in contact with water (Figure 9). The long-term water absorption capacity (equilibrium swelling ratio) tests of two different PA66 nanofibers in different solutions are shown in Figure 10. The water absorption of the two fiber samples increased sharply within the first 30 min, reaching the maximum value of 722% and 318% in

KCI solution and deionized water, respectively. This difference may be due to the presence of carboxyl groups in PAA in PAA-PA66 fiber and the alteration and pressurization of the internal system of water by salt ions, in which the activity of the fiber surface significantly improves the water absorption capacity [13]. For CF-PAA-PA66 fiber, the existence of its cross-linked structure not only implies the decrease of water absorption pores but also makes the membrane have higher water absorption resistance.

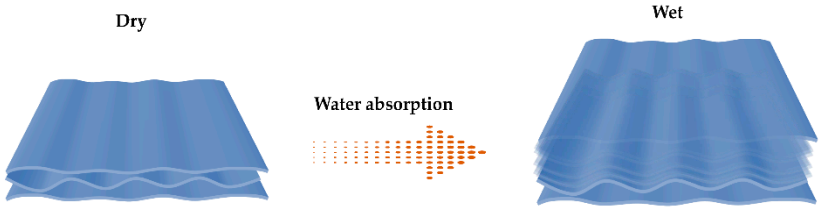

Figure 9. Expansion of nanofiber membrane matrix upon contact with water.

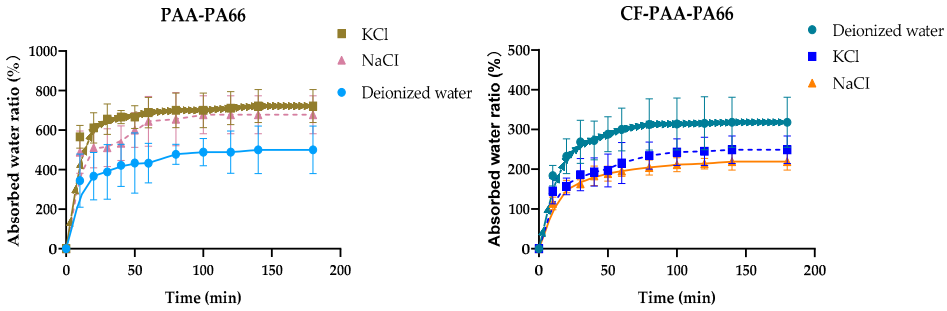

Figure 10. Water absorption swelling behavior of nanofibers.

Interestingly, the highly bio-absorbent swelling properties of uncrosslinked fiber could provide a promising solution for the development and application of cleaning products. Of course, cross-linked fibers also have a broad prospect of improving the waterproof properties of articles and clothing.

Figure 11 shows the fitting curves of the expansibility of related fiber membranes in PBS buffer at different incubation periods. Because of their high water permeability and strong water absorption, both fibrous membranes initially expand at a large swelling rate. The swelling degree of the fiber decreased as the solution consumed the fibers for a longer period of time. This is because, after a long time of immersion, the surface layer of the fiber membrane cracks itself or falls off with the matrix, which aggravates the local loss of the polymer matrix and leads to the medium in the buffer solution being leached out successively [27].

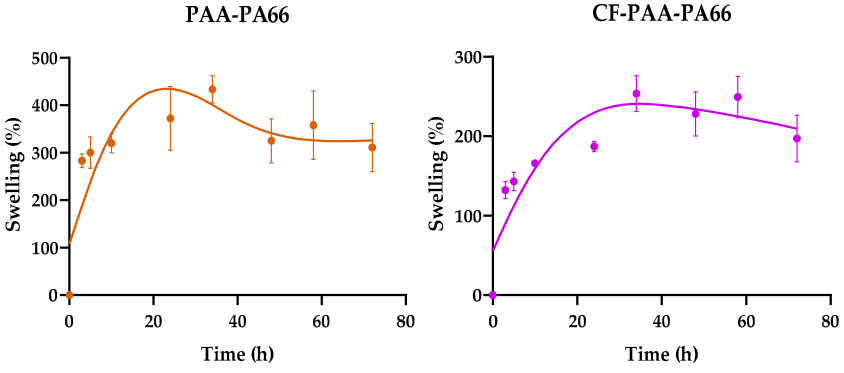

Figure 11. Swelling and expansion properties of fiber membranes in buffer solution for different curing times.

3.7. Permeability and Rejection Performance

To evaluate the separation and rejection performance of the fiber membranes, MTBE filtration experiments were performed. The results of permeability flux and MTBE rejection are shown in Figure 12a,b. The water flux values of the two fibers are 158.6 L/m^2·h and 26.8 L/m^2·h, respectively, but the stable rejection value is increased by 1.12 times. The further reduction of water flux with the involvement of the crosslinking reaction can be explained by the densification of the fiber membrane as a result of higher resistance to the permeation of water molecules [28]. Finally, the reduction in water flux of the CF-PAA-PA66 fiber membrane is also due to the combined effect of the presence of a large number of hydrophobic amide groups and the absence of hydrophilic carboxyl groups in the fiber.

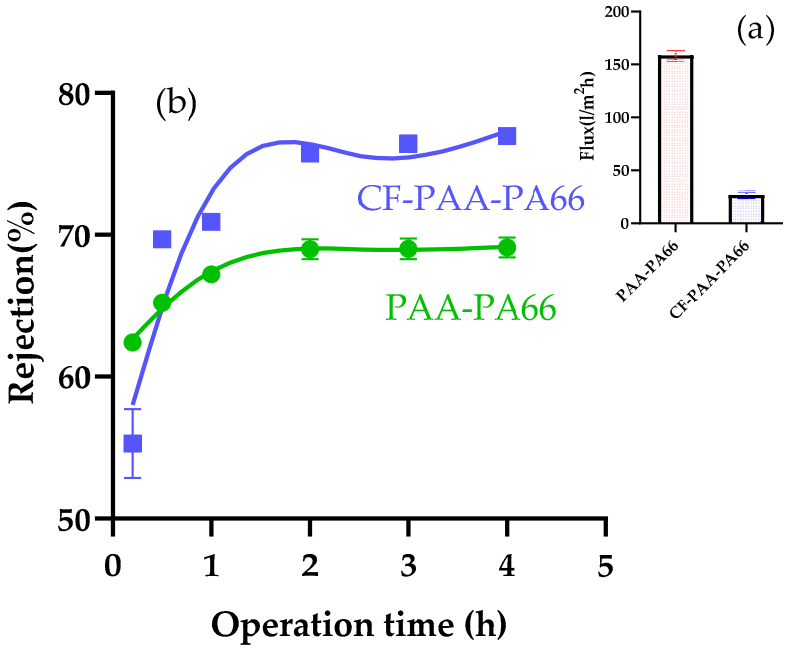

Figure 12. (**a**) Water flux and (**b**) MTBE rejection tested in MTBE solution.

Conversely, the rejection rates of MTBE increased with the increase of filtration time and eventually reached stable values of 69% and 77%, respectively. The two kinds of fiber membranes maintain relatively high rejection rates, which is attributed to the expansion and extension of fiber membranes in longitudinal space with the progress of the infiltration process, thus making the filtration path longer and increasing the pollutant retention time. Two kinds of fiber membrane screening mechanisms are shown in Figures 13 and 14, respectively. In addition, a hydration layer is formed at the interface between the aqueous phase and the membrane surface, which creates an energy barrier for the adsorption of pollutants.

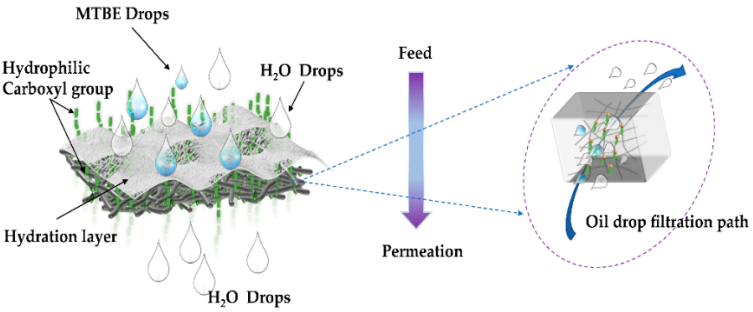

Figure 13. Filtration mechanism of PAA-PA66 fiber membrane.

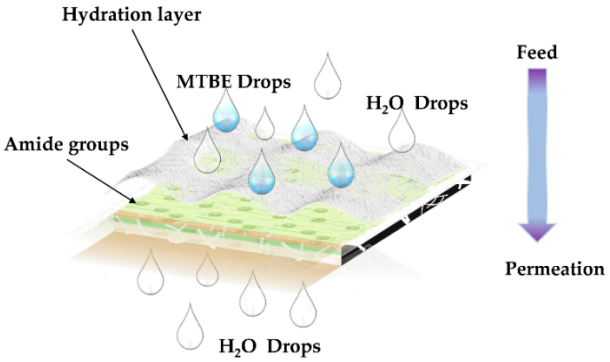

Figure 14. Filtration mechanism of CF-PAA-PA66 fiber membrane.

3.8. Mechanical Strength

The different spatial conformations and arrangements of nanofiber bundles in the fiber membrane directly affect the tensile properties of the membrane. Figure 15 shows the tensile test results of the nanofiber membranes. As can be seen, with the increase of breaking strain, the tensile strength difference of the fiber membrane before and after cross-linking becomes more and more prominent, which is 3.2 MPa and 1.4 MPa, respectively, and the breaking strain becomes smaller after cross-linking. This is due to the fact that the PA66 polymer chains in the cross-linking membrane are linear, while the PAA molecular chains at the new cross-linking point tend to exist as branched chains and the nanofibers are prone to direct lateral fracture. However, the nanofibers in the blended fiber membrane are uniformly stacked and arranged in the longitudinal direction and the nanofibers have higher bending elasticity, which leads to greater breaking strain [14].

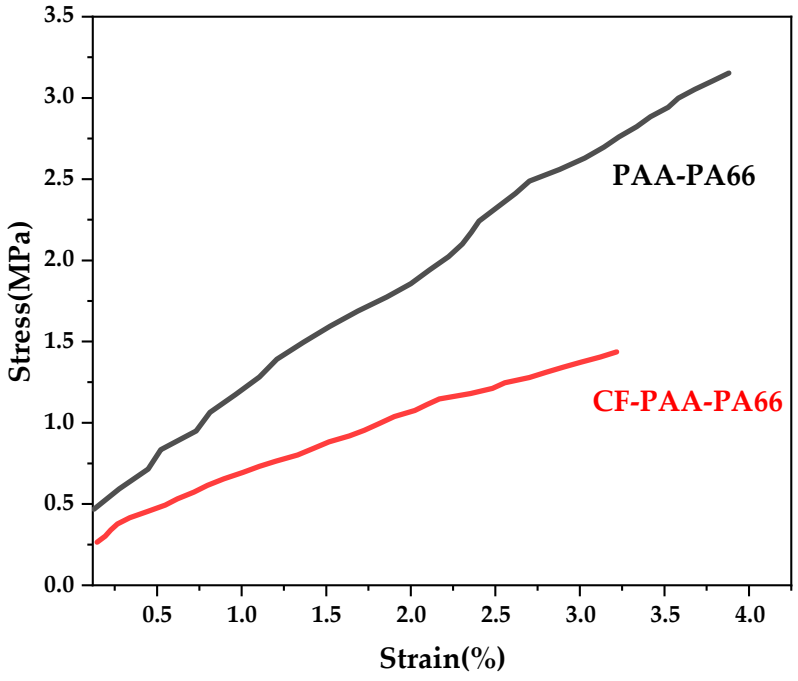

Figure 15. The stress–strain curves of PAA-PA66 and CF-PAA-PA66 fiber membranes.

4. Conclusions

A novel relatively porous to relatively dense non-porous membrane was developed.

Through the amidation reaction, PAA and PA66 are chemically cross-linked. Although the use of amidation activators such as EDC and NHS reduces the hydrophilicity of the fibrous membrane by reducing the reactive groups on the fiber surface, the generation

of covalent linkage with PA66 can improve the contaminant rejection rate of the fiber membrane and have high thermal stability and pH response stability while keeping the basic characteristics relatively unchanged. The results of aqueous solution absorption and radial filtration show that the process of permeation separation of two kinds of fiber membranes in solution is not only dominated by the ordinary screen interception effect, but also an important step that cannot be ignored is the longitudinal expansion and dilatation of fiber, which makes the interception path become curved and prolonged. In addition, the prepared PAA/PA66 nanocomposite can be applied to the cleaning of flexible articles and also for pretreatment of oily wastewater. As a result, the use of this modification method not only provides ideas for the establishment of a high chemical stability membrane skeleton structure but also can be applied to the mutual swelling polymerization between macromolecules.

Author Contributions: Conceptualization, J.Y. and B.W.; methodology, G.L.; software, W.W. (Wenxin Wu); validation, J.Y., B.W. and G.L.; formal analysis, B.W.; investigation, W.W. (Weixing Wu); resources, B.W.; data curation, Y.Z.; writing—original draft preparation, J.Y.; writing—review and editing, B.W.; visualization, M.G.; supervision, L.N.; project administration, B.W.; funding acquisition, J.Y. All authors have read and agreed to the published version of the manuscript.

Funding: This research was supported by Basic Public Welfare Research Program of Zhejiang Province (No. LGF19B070004 and LGF20E040002).

Institutional Review Board Statement: Not applicable.

Informed Consent Statement: Not applicable.

Data Availability Statement: The data used to support the findings of this study are available from the corresponding author upon request.

Acknowledgments: We also thank Lihong Nie for her donations of materials used for experiments.

Conflicts of Interest: The authors declare no conflict of interest.

References

1. Deitzel, J.M.; Kleinmeyer, J.; Harris, D.; Tan, N.B. The effect of processing variables on the morphology of electrospun nanofibers and textiles. *Polymer* **2001**, *42*, 261–272. [CrossRef]
2. Sas, I.; Gorga, R.E.; Joines, J.A.; Thoney, K.A. Literature review on superhydrophobic self-cleaning surfaces produced by electrospinning. *J. Polym. Sci. B Polym. Phys.* **2012**, *50*, 824–845. [CrossRef]
3. Tan, S.-H.; Inai, R.; Kotaki, M.; Ramakrishna, S. Systematic parameter study for ultra-fine fiber fabrication via electrospinning process. *Polymer* **2005**, *46*, 6128–6134. [CrossRef]
4. Pant, B.; Park, M.; Park, S.-J. Drug Delivery Applications of Core-Sheath Nanofibers Prepared by Coaxial Electrospinning: A Review. *Pharmaceutics* **2019**, *11*, 305. [CrossRef]
5. Li, D.; Xia, Y. Electrospinning of Nanofibers: Reinventing the Wheel? *Adv. Mater.* **2004**, *16*, 1151–1170. [CrossRef]
6. Lin, J.; Ding, B.; Yang, J.; Yu, J.; Sun, G. Subtle regulation of the micro- and nanostructures of electrospun polystyrene fibers and their application in oil absorption. *Nanoscale* **2012**, *4*, 176–182. [CrossRef]
7. Tobiesen, F.A.; Michielsen, S. Method for grafting poly (acrylic acid) onto nylon 6,6 using amine end groups on nylon surface. *J. Polym. Sci. A Polym. Chem.* **2002**, *40*, 719–728. [CrossRef]
8. Lu, L.; Yang, B.; Liu, J. Flexible multifunctional graphite nanosheet/electrospun-polyamide 66 nanocomposite sensor for ECG, strain, temperature and gas measurements. *Chem. Eng. J.* **2020**, *400*, 125928. [CrossRef]
9. Huang, Y.J.; Huang, C.L.; Lai, R.Y.; Zhuang, C.H.; Chiu, W.H.; Lee, K.M. Microstructure and Biological Properties of Electrospun In Situ Polymerization of Polycaprolactone-Graft-Polyacrylic Acid Nanofibers and Its Composite Nanofiber Dressings. *Polymers* **2021**, *13*, 4246. [CrossRef]
10. Yan, J.; Nie, L.; Li, G.; Zhu, Y.; Gao, M.; Wu, R.; Wang, B. Graphene Oxide Modified Polyamide 66 Ultrafiltration Membranes with Enhanced Anti-Fouling Performance. *Membranes* **2022**, *12*, 458. [CrossRef]
11. Zeng, J.; Hou, H.; Wendorff, J.H.; Greiner, A. Electrospun poly (vinyl alcohol)/poly (acrylic acid) fibres with excellent water-stability. *E-Polymers* **2004**, *4*, 899. [CrossRef]
12. Park, Y.; Lee, S.; Ha, S.S.; Alunda, B.; Noh, D.Y.; Lee, Y.J.; Kim, S.; Seol, J.H. Crosslinking Effect on Thermal Conductivity of Electrospun Poly (acrylic acid) Nanofibers. *Polymers* **2019**, *11*, 858. [CrossRef] [PubMed]
13. Ranjbari, E.; Bazgir, S.; Shirazi, M.M.A. Needleless electrospinning of poly (acrylic acid) superabsorbent: Fabrication, characterization and swelling behavior. *Polym. Test.* **2020**, *84*, 106403. [CrossRef]

14. Wu, S.; Wang, B.; Zheng, G.; Liu, S.; Dai, K.; Liu, C.; Shen, C. Preparation and characterization of macroscopically electrospun polyamide 66 nanofiber bundles. *Mater. Lett.* **2014**, *124*, 77–80. [CrossRef]
15. Li, L.; Hsieh, Y.-L. Ultra-fine polyelectrolyte fibers from electrospinning of poly (acrylic acid). *Polymer* **2005**, *46*, 5133–5139. [CrossRef]
16. Gao, Y.; Sang, X.; Chen, Y.; Li, Y.; Liu, B.; Sheng, J.; Feng, Y.; Li, L.; Liu, H.; Wang, X.; et al. Polydopamine modification electrospun polyacrylonitrile fibrous membrane with decreased pore size and dendrite mitigation for lithium ion battery. *J. Mater. Sci.* **2019**, *55*, 3549–3560. [CrossRef]
17. Yan, J.; Huang, Y.; Miao, Y.E.; Tjiu, W.W.; Liu, T. Polydopamine-coated electrospun poly (vinyl alcohol)/poly (acrylic acid) membranes as efficient dye adsorbent with good recyclability. *J. Hazard. Mater.* **2015**, *283*, 730–739. [CrossRef]
18. Huang, Y.L.; Baji, A.; Tien, H.W.; Yang, Y.K.; Yang, S.Y.; Ma, C.C.; Liu, H.Y.; Mai, Y.W.; Wang, N.H. Self-assembly of graphene onto electrospun polyamide 66 nanofibers as transparent conductive thin films. *Nanotechnology* **2011**, *22*, 475603. [CrossRef]
19. Kim, B.; Park, H.; Lee, S.-H.; Sigmund, W.M. Poly (acrylic acid) nanofibers by electrospinning. *Mater. Lett.* **2005**, *59*, 829–832. [CrossRef]
20. Han, W.; Zheng, G.; Liang, Y.; Dai, K.; Liu, C.; Chen, J.; Shen, C.; Peng, X.; Fu, P.; Cao, W.; et al. HDPE solution crystallization induced by electrospun PA66 nanofiber. *Colloid Polym. Sci.* **2011**, *289*, 843–848. [CrossRef]
21. Poletto, P.; Duarte, J.; Thürmer, M.B.; Santos, V.d.; Zeni, M. Characterization of Polyamide 66 membranes prepared by phase inversion using formic acid and hydrochloric acid such as solvents. *Mater. Res.* **2011**, *14*, 547–551. [CrossRef]
22. Chang, X.; Wang, Z.; Quan, S.; Xu, Y.; Jiang, Z.; Shao, L. Exploring the synergetic effects of graphene oxide (GO) and polyvinylpyrrodione (PVP) on poly (vinylylidenefluoride) (PVDF) ultrafiltration membrane performance. *Appl. Surf. Sci.* **2014**, *316*, 537–548. [CrossRef]
23. Xiang, S.; Guo, Z.; Wang, Y.; Liu, H.; Zhang, J.; Cui, Z.; Wang, H.; Li, J. The microstructure regulation, strengthening, toughening and hydrophilicity of polyamide6 in fabricating poly (vinylidene fluoride)-based flat membrane via the thermally induced phase separation technique. *Eur. Polym. J.* **2020**, *126*, 109568. [CrossRef]
24. Cui, Z.; Hassankiadeh, N.T.; Lee, S.Y.; Lee, J.M.; Woo, K.T.; Sanguineti, A.; Arcella, V.; Lee, Y.M.; Drioli, E. Poly (vinylidene fluoride) membrane preparation with an environmental diluent via thermally induced phase separation. *J. Membr. Sci.* **2013**, *444*, 223–236. [CrossRef]
25. Chao, S.; Li, X.; Li, Y.; Wang, Y.; Wang, C. Preparation of polydopamine-modified zeolitic imidazolate framework-8 functionalized electrospun fibers for efficient removal of tetracycline. *J. Colloid Interface Sci.* **2019**, *552*, 506–516. [CrossRef]
26. Kang, H.-K.; Shin, H.-K.; Jeun, J.-P.; Kim, H.-B.; Kang, P.-H. Fabrication and characterization of electrospun polyamide 66 fibers crosslinked by gamma irradiation. *Macromol. Res.* **2011**, *19*, 364–369. [CrossRef]
27. Ekram, B.; Abd El-Hady, B.M.; El-Kady, A.M.; Amr, S.M.; Gabr, H.; Waly, A.I.; Guirguis, O.W. Enhancing the Stability, Hydrophilicity, Mechanical and Biological Properties of Electrospun Polycaprolactone in Formic Acid/Acetic Acid Solvent System. *Fibers Polym.* **2019**, *20*, 715–724. [CrossRef]
28. Zhang, L.; Han, N.; Tan, L.; Qian, Y.; Cui, Z.; Cai, J. Preparation of hydrolysis of poly (acrylonitrile-co-methyl acrylate) membranes via thermally induced phase separation: Effects of hydrolysis conditions and additives. *J. Appl. Polym. Sci.* **2018**, *135*, 46380. [CrossRef]